Pure Appl. Chem., Vol. 78, No. 1, pp. 45–64, 2006.
doi:10.1351/pac200678010045

Solution-based routes to transition-metal oxide one-dimensional nanostructures*

Xun Wang‡ and Yadong Li

Department of Chemistry, Tsinghua University, Beijing 100084, China

Abstract: One-dimensional (1D) nanostructures have drawn continuous research attention because of their unique electrical, optical, and magnetic properties different from that of bulk and nanoparticles, as well as their potential applications in mesoscopic research and nanodevices. The main challenge in this area is how to precisely control the sizes, dimensionalities, compositions, and crystal structures in nanoscale, which may serve as a powerful tool for the tailoring of physical/chemical properties of materials in a controllable way. Here, we review the advances in the solution-based routes to prepare 1D nanostructures. Particularly, three systems of MnO_2, rare-earth compounds, and silicates have been chosen to show the synthetic strategy under hydrothermal conditions. As the main theme, a rolling mechanism has been given special attention to present a relative general understanding of the growth of various transition-metal oxide (TMO) 1D nanostructures under solution conditions.

Keywords: particle synthesis; 1D nanostructures; solution-based routes; rolling mechanism; transition-metal oxides.

INTRODUCTION

In 1959, Richard Feynman described the problems of manipulating and controlling things on a small scale and predicted that there is plenty of room at the bottom [1], which, as the central idea of nanoscience and nanotechnology, has long been the pursuit of scientists worldwide. In the past decades, the development of various chemical or physical methods have enabled us to partly fulfill this goal [2–15], based on which many new and promising fields have been established, including nanofabrication, nanodevices, nanobiology, and nanocatalysis, etc. Among all kinds of nanosystems such as zero- [2], one- [3–4], and two-dimensional [5] systems, one-dimensional (1D) nanostructures are particularly interesting in that they usually have diameters in nanometer scale and lengths in micro- and/or even macroscale, the controlled growth of which involves the breaking of crystal symmetry and are quite different from the general concept of crystal growth [6]. So if we can gain the general principle in controlled growth of 1D nanostructures, that is, why the atoms can self-assemble in such a way and what are the driving force in this process, it is most probable that we will make great progress toward manipulating and controlling atoms at the nanoscale and thus drive more opportunities to this fast-expanding research field.

Besides physical methods such as physical vapor deposition and scanning tunneling microscopy (STM) manipulation, etc., chemical methods that usually start from atomic-level precursors and result in new compounds with the formation of new chemical bonding, play important roles in controlled syn-

Pure Appl. Chem.* **78, 1–64 (2006). A collection of invited, peer-reviewed articles by the winners of the 2005 IUPAC Prize for Young Chemists.

‡Corresponding author: E-mail: wangxun@mail.tsinghua.edu.cn

thesis of nanomaterials [13–23]. By properly tuning factors such as precursors, chemical potential, temperature, and concentration, the rearrangement and bonding of atoms can be rationally tuned in a desirable way, and results in structures with designated composition, crystal structures, sizes, and dimensionalities. As for the synthesis of 1D nanostructures, emphasis has been placed on the ways that the chemical reactions will occur to ensure the anisotropic growth of the nanocrystals. For example, by adopting anodic aluminum oxide (AAO) as templates, the reactions can be controlled to take place in the confined spaces and the growth of nanostructures will follow the shape and sizes of the original templates [10]; in a typical vapor–liquid–solid growth process, by employing metal clusters as catalysts, the absorption of the monomers, and the subsequent chemical reaction and/or crystal growth processes can proceed with the liquid clusters as energetic favorable sites, which may provide the driving force for the anisotropic growth of the as-obtained 1D nanostructures [4].

Compared with the template-confined and very large-scale (VLS) growth procedure, solution-based routes, although evidenced to be effective in generating 1D nanostructures, are more complex: numerous factors such as temperature, concentration, pH conditions, crystal structures, precursors, inorganic additives, solvents, and surfactants, together with catalysts and other dynamic parameters, are reported to have influence on the growth behavior of the nanocrystals, which present great difficulty in investigating the driving force and the underlying principles. Since the solution-based routes are quite general in preparing all kinds of nanostructures and usually have the advantages of flexibility and large-scale production, it would be quite fundamental to investigate the general formation mechanism of 1D nanostructures under solution conditions. In this review, we will focus on the controlled synthesis of transition-metal oxide (TMO) 1D nanostructures under hydrothermal conditions. Although the above-mentioned numerous parameters may influence the growth of nanocrystals, crystal structure as the inherent factor that may determine the growth behavior of the nanocrystals was emphasized, and compounds with layer structures are given special attention in that they are often found related to the growth of 1D nanostructures, including nanowires and nanotubes. In most of the summarized cases, aqueous systems were adopted and the uses of surfactants were avoided to simplify the reaction systems (although in some reports, nonaqueous solvents and appropriate capping reagents do assist the growth of 1D nanostructures), which may give us a clearer picture of the decisive factors.

LAYER STRUCTURES IN TRANSITION-METAL OXIDES AND THEIR ASSOCIATION WITH THE CONTROLLED GROWTH OF ONE-DIMENSIONAL NANOSTRUCTURES

Oxides are the most commonly seen minerals in the earth and have now been widely used in various areas, from ceramics, catalysis, sensor, to electronics, optics, and magnetic fields. With reduced dimensionalities, more new and exciting physical and chemical contains were discovered, for example, room-temperature ultraviolet nanolasers [24], subwavelength waveguides [25], and room-temperature nanosensors [26]. In the past few years, we have endeavored to develop a solution-based route to get TMO 1D nanostructures via a rolling mechanism [16–23], the basic concept of which is that layer (natural or artificial) structures may roll from the edges under elevated temperature and pressure and the as-obtained tubular structures may serve as the original driving force for the growth of 1D nanostructures.

This inspiration originates from the synthesis of carbon and other inorganic nanotubes. Besides carbon, nanotubes such as $B_xC_yN_z$ [27], MS_2 (M = Mo, W, Nb, Ta, etc.) [28], $NiCl_2$ [29], vanadium oxide [30], and Bi [16] have been synthesized under favorable conditions. Similar to graphite carbon, all these compounds have layer structures in their bulk crystals, and the layers are held together mainly by weak van der Waals' forces. A clear understanding about the bending of the graphite under high temperature or electron beam irradiation has been elucidated [31], which further strengthens the possibility of the rolling process of a lamellar structure. A rational assumption is now that the graphite sheets can roll into tubes, other inorganic layered structure materials might behave in a similar way. This as-

sumption was experimentally testified in the preparation of WS_2 nanotubes via artificial organic–inorganic lamellar structures as intermediates [18], and further evidenced in the controlled decomposition of layered ME.0.5en (M = Cd, Zn, E = S, Se) into ME nanorods [32].

Since layer structures are quite common in TMOs, such as δ-MnO_2, titanate, $K_4Nb_6O_{17}$, silicates, MoO_3, V_2O_5, and various hydroxides, etc., it is possible to prepare new-type 1D nanostructures from these two-dimensional (2D) layered structures, and most importantly, phase transformation from layer to other nonlayer structures may occur under controlled experimental conditions, so that 1D nanostructures of other three-dimensional (3D) structured compounds might be obtained via 2D structures as intermediates.

In this manuscript, three systems of MnO_2 [33–36], rare-earth compounds [37–41], and silicates [42–43] have been reviewed to show the whole picture of from layer-structured compounds to 1D nanostructures of TMO under hydrothermal conditions.

MANGANESE DIOXIDE NANOWIRES AND NANOTUBES

Manganese dioxides and derivative compounds have received intense attention, because of their outstanding structural flexibility combined with novel chemical and physical properties, which are of interest for the following applications, for example, molecular sieves, catalysts, and Li/MnO_2 batteries [44–50]. Different structural forms of MnO_2 exist in nature, such as the α, β, γ, and δ-types. Different forms of MnO_2 are exactly based on the same structural units [MnO_6] octahedral. α-, β-, γ-MnO_2 have [MnO_6] chains in their structures, and are typical of 1×1, 2×2, 1×2 1D channels, respectively, while δ-type is well known for its layer structure, which is composed of edge-sharing [MnO_6] octahedral [44]. Among the several crystallographic forms of MnO_2, δ-MnO_2 alone has a layer structure, which is indispensable in the rolling mechanism. So studies have been focused on the roles δ-MnO_2 playing in the formation of the other structural MnO_2 1D nanostructures.

On the basis of the redox reactions of MnO_4^- and/or Mn^{2+}, a rational low-temperature hydrothermal chemical synthetic way has been developed to selectively prepare MnO_2 nanowires/nanotubes with different crystal structures, including α-, β-, γ-, and δ-MnO_2 [35]. The structural stability of different structures has been fully discussed, and the transformation between different crystal structures has been established (Fig. 1) based on experiment results. The layer-structured δ-MnO_2 is especially found to be the intermediate for the formation of MnO_2 1D nanostructures, based on which a rolling mechanism from layer-structured δ-MnO_2 to MnO_2 nanowires/nanotubes with different structures has been introduced to explain the growth of MnO_2 nanowires/nanotubes under hydrothermal conditions. By properly designing redox reactions in Mn-related chemical species, the chemistry in the MnO_2-related system has been successfully applied in the precisely controlled synthesis of MnO_2 low-dimensional nanostructures.

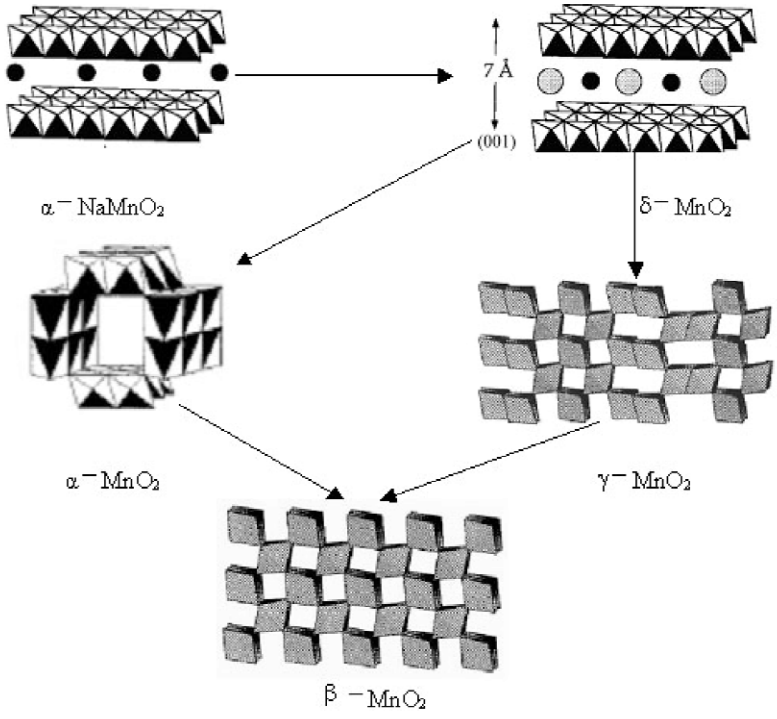

Fig. 1 Crystal structure of manganese dioxides and manganese α-$NaMnO_2$.

As shown in Fig. 2, based on experiment results, different crystal forms of MnO_2 can be obtained via layer-structured δ-MnO_2 as intermediate. And the key to the structure stability would be the concentration of the cation like NH_4^+ and K^+.

Two strategies of Mn^{2+} oxidized into MnO_2 and MnO_4^- reduced into MnO_2 have been employed:

$$MnO_2 + 4H^+ + 2e \rightarrow Mn^{2+} + H_2O \ (E^\circ = 1.23 \ \text{V}) \quad (1)$$

$$MnO_4^- + 4H^+ + 3e \rightarrow MnO_2 + 2H_2O \ (E^\circ = 1.695 \ \text{V}) \quad (2)$$

$(NH_4)_2S_2O_8$ has been used as the oxidizing reagent for reaction 1 to proceed.

Since different types of MnO_2 are close in structures, the reaction conditions for selected controlled synthesis are almost the same, except for the ion concentrations. Experiment results show that different tunnel structures need different amounts of ions to stabilize.

Under hydrothermal conditions, α- and β-MnO_2 have been obtained by varying the concentration of NH_4^+ and SO_4^{2-}. The final products of direct reaction of $(NH_4)_2S_2O_8$ and $MnSO_4$ is β-MnO_2 (Fig. 2B), however, if the direct reaction occurs at 90 °C, 1 atm, γ-MnO_2 nanorods will be obtained. The phase will change to α-MnO_2 (Fig. 2A) when a certain amount of $(NH_4)_2SO_4$ is introduced to the reaction system. In this process, it is apparent that the 2×2 tunnel structures need more NH_4^+ ions to stabilize than 1×1 tunnels.

$KMnO_4$ has also been used as oxidizing reagents of $MnSO_4$. The molar ratios of $KMnO_4$ and $MnSO_4$ were varied in order to prepare MnO_2 nanorods with different crystallographic forms. δ-MnO_2 nanorods have been obtained when pure $KMnO_4$ or a high mole ratio (around 6:1) $KMnO_4/MnSO_4$ mixture is hydrothermal treated at 140 °C. When the mole ratio of $KMnO_4/MnSO_4$ is controlled at about 2:1, the products are examined to be α-MnO_2 nanorods. When the mole ratio is adjusted to around 2:3, the reaction will result in β-MnO_2 nanorods. It is believed that K^+ cation concentration in different reaction systems is responsible for the formation of different crystal structures of MnO_2 [35].

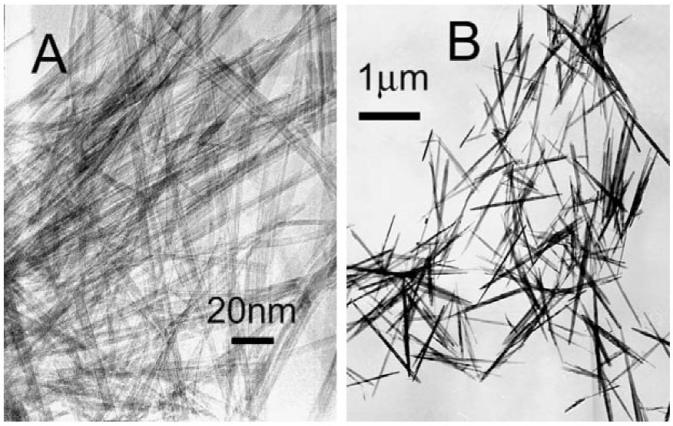

Fig. 2 TEM images of α-MnO_2 and β-MnO_2 (adapted from [35]).

Although the Mn sources are different, all the MnO_2 nanowires have undergone a similar growing process. As shown in Figs. 3A and 4B, the X-ray diffraction (XRD) patterns of α-MnO_2 in a $(NH_4)_2S_2O_8$–$MnSO_4$ reaction system, taken after 30 min hydrothermal treatment, can be readily indexed to that of δ-MnO_2 and all the samples show lamellar structure morphologies. When the reaction time is prolonged, lots of nanotubes have been observed existing in the intermediate (Fig. 3D). However, after a further prolonged reaction time (1.5 h), the nanotubes will disappear, only nanowires can be obtained, and the XRD patterns (Fig. 4A) of the samples have shown a great similarity to that of α-MnO_2 with less crystallinity.

Similar XRD patterns of δ-MnO_2 have also been obtained from the intermediate (after 1 h) of α-MnO_2 in a $KMnO_4$–$MnSO_4$ reaction system or intermediate of δ-MnO_2 ($KMnO_4$ hydrothermal for 2 h). Transmission electron microscopy (TEM) images of the samples also take on a look of lamellar and curling structures. The information indicates that although α-MnO_2 has resulted from different synthetic methods, they have undergone a similar growth process. Further studies have also evidenced a rolling process for the growth of β-MnO_2 nanorods [$(NH_4)_2S_2O_8$–$MnSO_4$ system as well as $KMnO_4$–$MnSO_4$ reaction system], however, a different phase transformation process: δ → α → β [$(NH_4)_2S_2O_8$–$MnSO_4$ system], δ → γ → β ($KMnO_4$–$MnSO_4$ reaction system) [35].

Based on the above experiment results, all the MnO_2 1D nanostructures have undergone a common developing process, which is characteristic of the rolling mechanism and phase transformation.

This rolling strategy has been further evidenced in the controlled synthesis of δ-MnO_2 nanotubes via α-$NaMnO_2$ as precursors [36]. Based on the MnO_2 nanowires/nanorods studies, the [MnO_6] octahedral layers in δ-MnO_2 could be easily exfoliated and tend to curl under hydrothermal conditions, which have provided the possibility for the formation of δ-MnO_2 nanotubes [10]. Rational precursors and favorable conditions may facilitate this formation process. Among the numerous manganese oxides, α-$NaMnO_2$ (sodium manganese oxide) is layered and adopts a monoclinic distortion of the $LiCoO_2$ structure caused by the Jahn–Teller activity of Mn^{3+}. Na^+ ions reside between edge-shared [MnO_6] octahedra layers in $NaMnO_2$ (Fig. 1) [11–12]. The strong static interaction between the Na^+ ions and [MnO_6] units hold the layers together tightly and make it impossible for these layers to roll up into nanotubes. However, the layer-structured α-$NaMnO_2$ has proven to be an ideal precursor for the formation of δ-MnO_2 nanotubes.

Under a neutral pH condition, Mn^{3+} is unstable and disproportionation reaction will occur,

$$Mn^{3+} \rightarrow Mn^{2+} + MnO_2 \ (E^\circ = +0.56 \text{ V}; \ \Delta G^\circ = -54.04 \text{ kJ mol}^{-1})$$

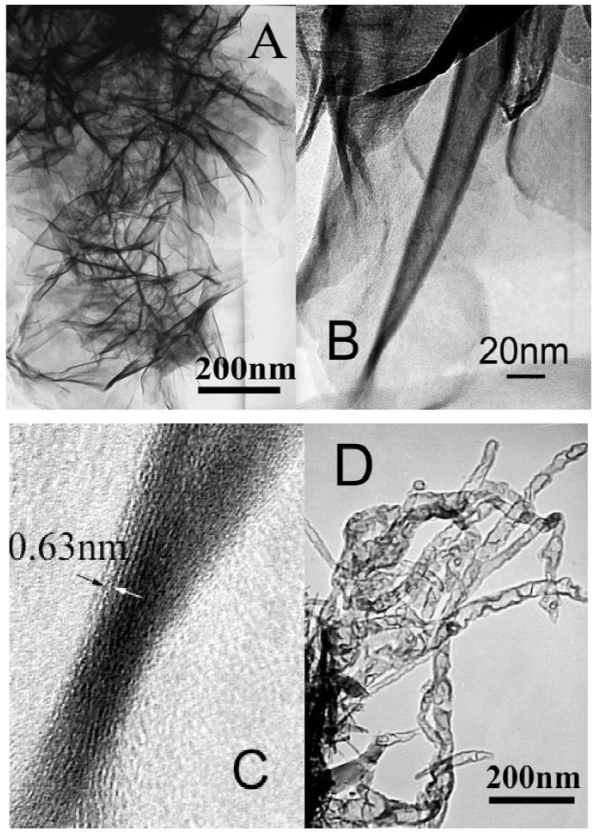

Fig. 3 (A) TEM image of the α-MnO_2 intermediate [$(NH_4)_2S_2O_8$–$MnSO_4$ reaction system] after hydrothermal treatment for 30 min; (B) High-resolution TEM (HRTEM) image of the curling intermediate after hydrothermal treatment for 30 min; (C) HRTEM image of the corresponding part in Fig. 3B; (D) TEM image of the α-MnO_2 tubular intermediate after hydrothermal treatment for 45 min (adapted from [35]).

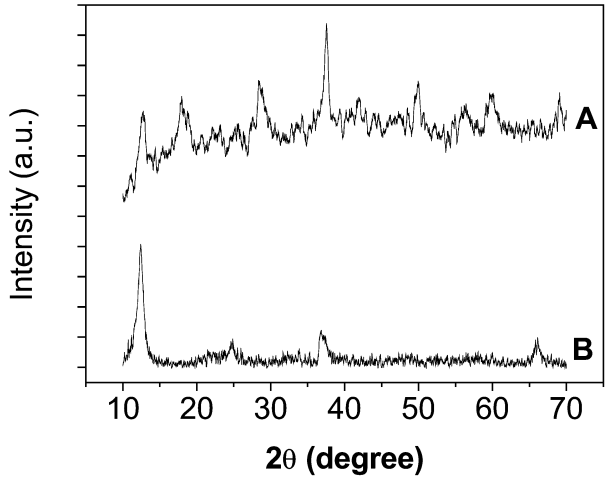

Fig. 4 (A) XRD patterns of the α-MnO_2 intermediate [$(NH_4)_2S_2O_8$–$MnSO_4$ system] after hydrothermal treatment for 2 h; (B) XRD patterns of the α-MnO_2 intermediate [$(NH_4)_2S_2O_8$–$MnSO_4$ system] after hydrothermal treatment for 30 min.

Along with this process, Na^+ ions will be released, and the $NaMnO_2$ can be gradually intercalated by water molecular with part of the Mn^{3+} transformed into Mn^{4+} [11], which will in situ adopt [MnO_6] octahedral to form manganese oxide layers with H_2O intercalated. As a result, the interlayer distance will be enlarged, so the strong static interaction between the MnO_6 octahedra sheets would be weakened to some extent, which might lower the energy barrier in turning into tubular morphology, and thus greatly increase the possibility for the formation of δ-MnO_2 nanotubes (Fig. 5).

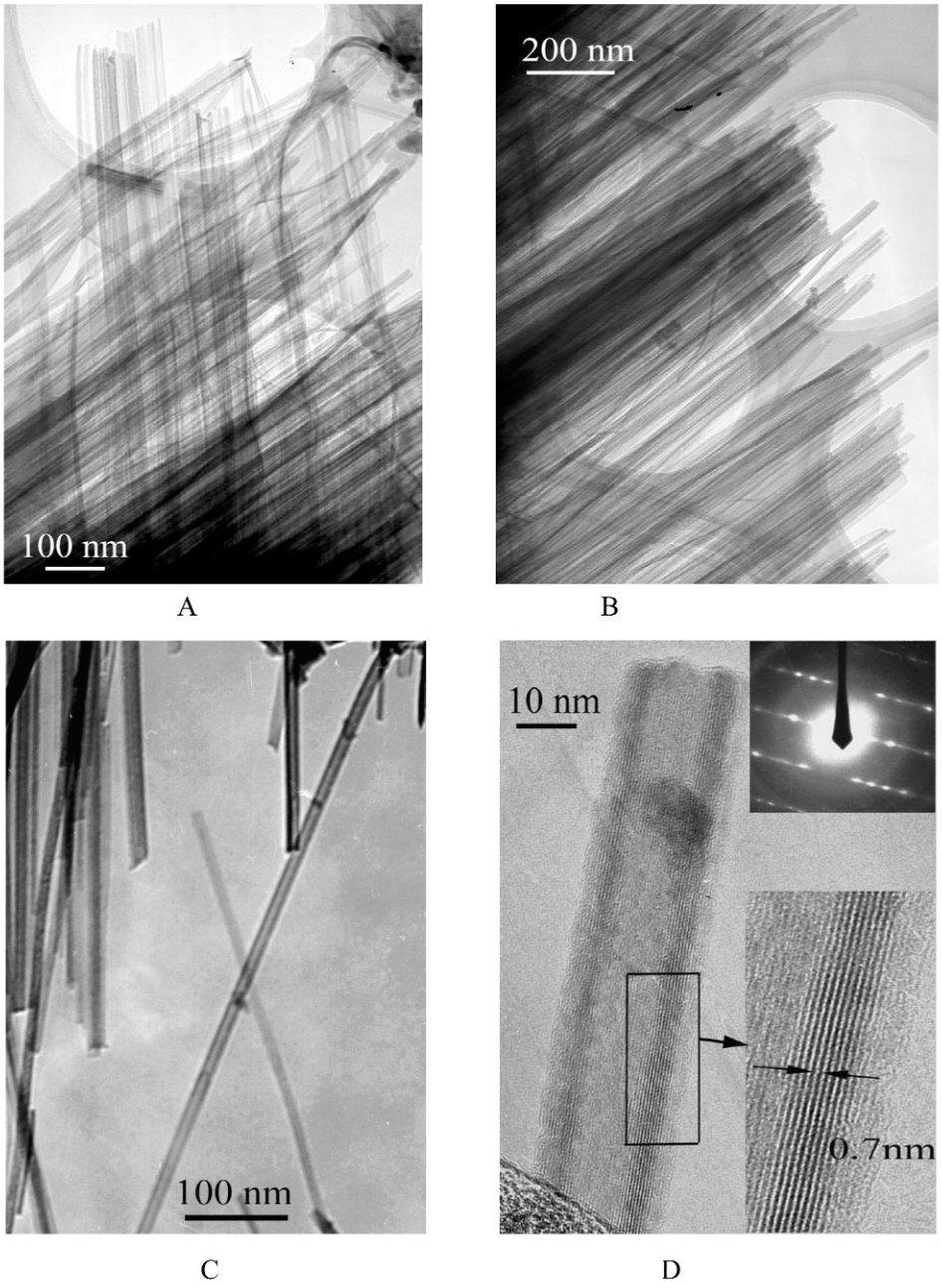

Fig. 5 TEM images of δ-MnO_2 nanotubes with α-$NaMnO_2$ as precursors (adapted from [36]).

The synthesis of MnO_2 nanowires/rods and nanotubes, together with other non-oxide compounds such as Bi nanotubes, show that the rolling mechanism may be a general method for the synthesis of nanowires/nanotubes from natural lamellar structures under aqueous conditions.

As an example, the successful synthesis of MnO_2 nanowires/rods and nanotubes also show that it is convenient to control the crystal structure or oxidation state of the final products by properly selecting the reducing or oxidizing reagents and the reaction conditions, which may be the major advantages of the solution-based method.

RARE-EARTH COMPOUND NANOWIRES, NANOTUBES, AND FULLERENE-LIKE NANOPARTICLES

Apart from the MnO_2 species, there exist no layer-structured compounds that may serve as intermediates for the formation of rare-earth 1D nanostructures. The synthesis of lanthanide hydroxide nanowires was inspired from their crystal structures [37]. As far as the obtained $Ln(OH)_3$ nanowires are concerned, they all have a hexagonal crystal structure, just like that of ZnO, which is well known for its anisotropic growth nature. However, when investigating the formation process of these nanowires, especially the influences of pH on the morphology evolution of the nanostructures, some sheet structures are obtained, which show that the hexagonal-structured hydroxides can grow in a 2D mode under desired conditions. So the question is: whether or not these nontypical 2D compounds can be prepared as nanotubes that are usually prepared from 2D layer structures [38]. This assumption was confirmed by the formation of hydroxide nanotubes [39] under a lower-temperature condition than that of nanowires (Fig. 6).

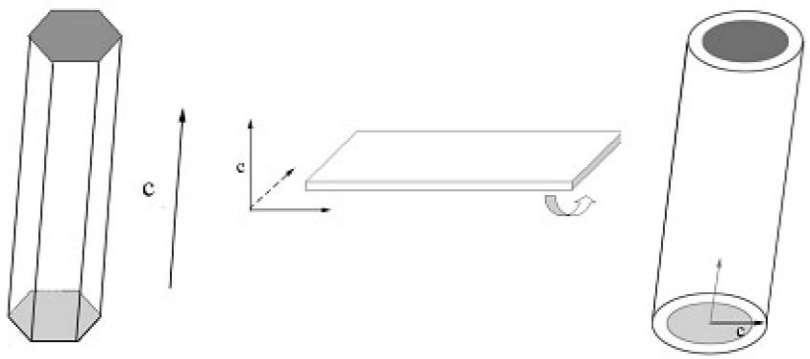

Fig. 6 Illustration of the growth modes of hexagonal lanthanide hydroxides under different experimental conditions.

The synthesis of $Ln(OH)_3$ nanowires (Fig. 7) was based on the preparation of colloidal $Ln(OH)_3$ at room temperature, and the subsequent hydrothermal treatment at 180 °C for about 12 h, while the preparation of hydroxide nanotubes (Fig. 8) was carried out at lower-temperature conditions of from 120–140 °C. The similar experiment conditions provide an ideal system for the investigation of the formation of nanowires or nanotubes.

It is interesting to find that, under controlled experimental conditions, the different lighter $Ln(OH)_3$ ($La(OH)_3$, $Pr(OH)_3$, $Nd(OH)_3$, $Sm(OH)_3$, $Eu(OH)_3$, and $Gd(OH)_3$ nanowires could be prepared as high-aspect-ratio products with similar outlook, while, under the same conditions, heavier lanthanide hydroxide—$Dy(OH)_3$, $Tb(OH)_3$, $Ho(OH)_3$, $Tm(OH)_3$, and YbOOH—usually have lower aspect ratios or less uniform morphologies. And for the hydroxide nanotubes, light lanthanide compounds usually have smaller diameters, while the heavy lanthanide hydroxides can be prepared as nanotubes with larger diameters.

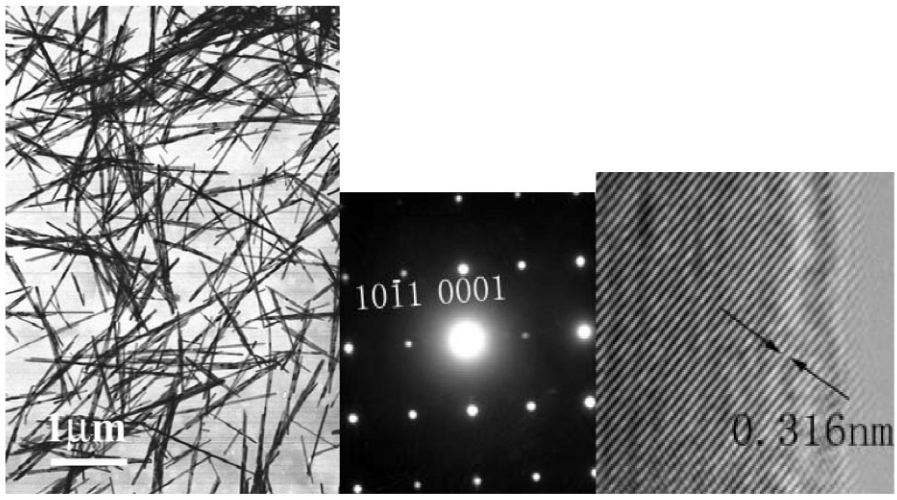

A B C

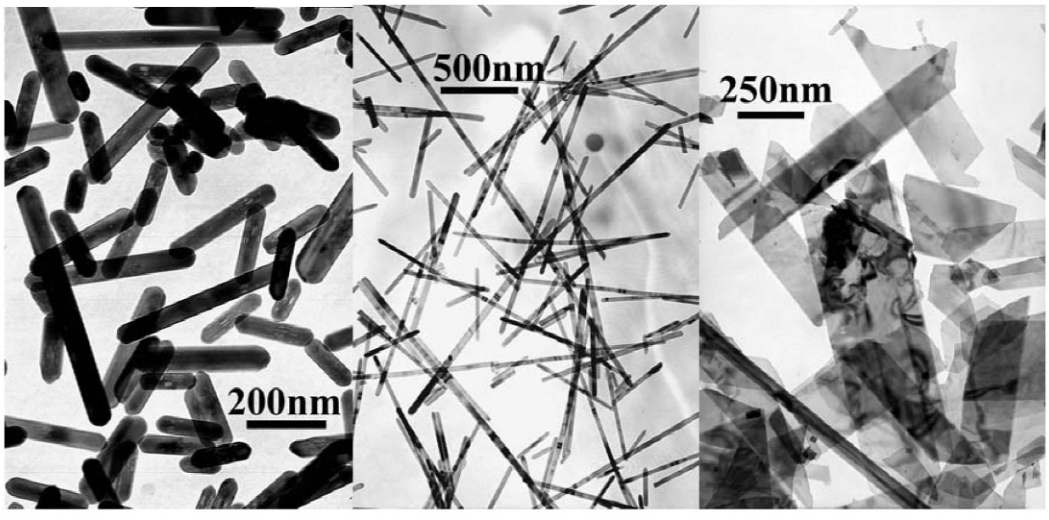

D E F

Fig. 7 (A) TEM images of $La(OH)_3$ nanowires (KOH 5 mol/l); (B) electron diffraction patterns of a single $La(OH)_3$ nanowire; (C) HRTEM images taken from a single $La(OH)_3$ nanowire; (D) TEM images of $Sm(OH)_3$ nanosheets, pH = 6~7; (E) TEM images of $Sm(OH)_3$ nanowires, pH = 9~10; (F) TEM images of $Sm(OH)_3$ nanorods, KOH, 5 mol/l (adapted from [37]).

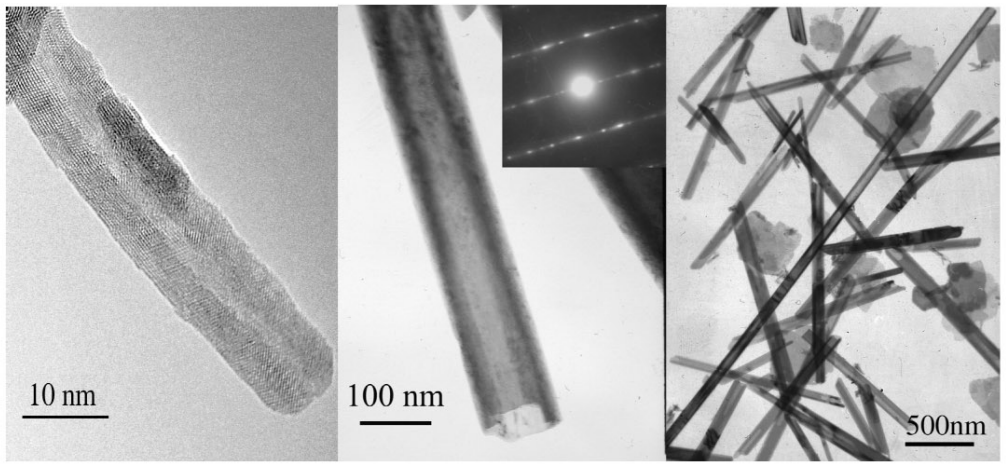

A B C

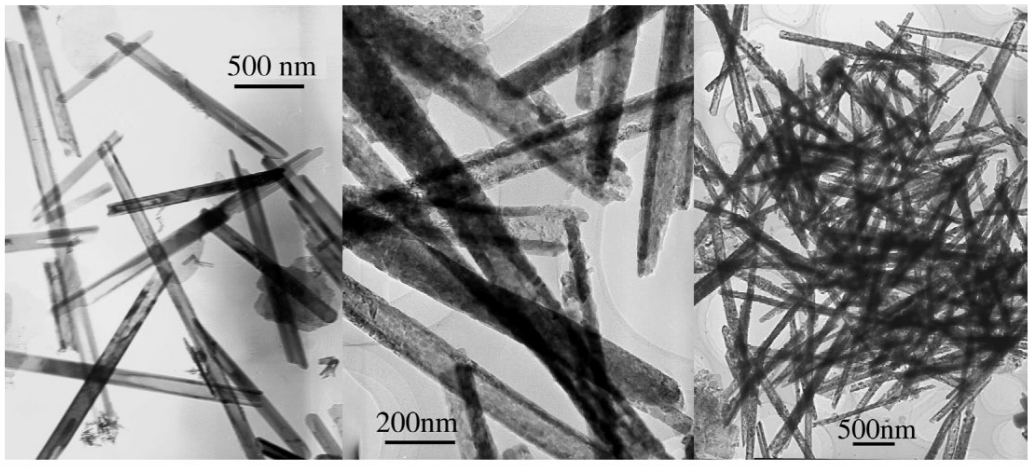

D E F

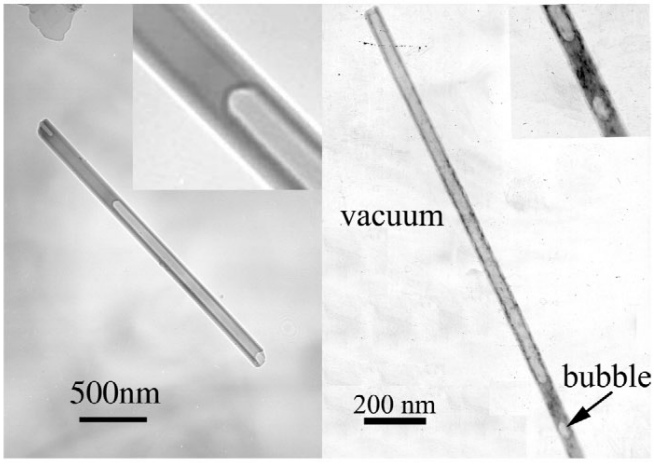

G H

(*continues on next page*)

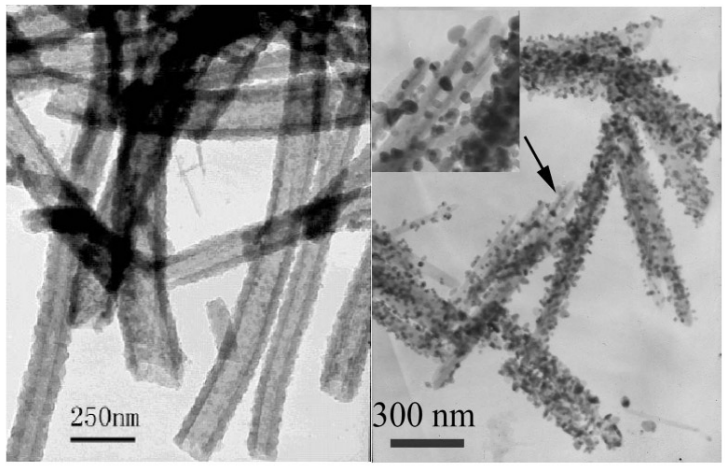

Fig. 8 (A) HRTEM images of an individual $Eu(OH)_3$ nanotubes; (B) TEM images of an individual $Er(OH)_3$ nanotube with an open end; (C) TEM images of $Dy(OH)_3$ nanotubes; (D) TEM images of $Y(OH)_{2.14}F_{0.86}$ nanotubes; (E,F) TEM images of Y_2O_2S nanotubes; (G,H) individual nanotube of $Y(OH)_3$ containing ethanol inside; (I) TEM images of $Y(OH)_3$–MMA nanotubes; (J) TEM images of $Y(OH)_3$ nanotubes decorated with Au nanoparticles (adapted from [37,39,40]).

With the decreasing of the ion radii (from La to Lu), under the adopted experimental conditions, the crystal structure of lanthanide hydroxides gradually changes from a typical hexagonal phase [$La(OH)_3$] to a monoclinic one [$Lu(OH)_3$], which results in the formation of monoclinic YbOOH instead of hexagonal $Yb(OH)_3$ in high-temperature experimental conditions (nanowire synthesis, 180 °C); along with this change, the tendency to grow along certain direction has been weakened to some extent, so the heavier lanthanide hydroxide nanowires usually have lower aspect ratios and less uniform morphologies. The diameters of the hydroxide nanotubes might be determined by the rigidity of the corresponding layers of different hydroxides.

Further investigation can be carried out on the growth dynamics of $Ln(OH)_3$ nanowires/nanotubes, which may serve as a perfect model to study the crystallization in nanoscale since they have similar and gradually changing crystal structures.

Similar precipitation–hydrothermal methods have been applied in the synthesis of rare-earth fluoride inorganic fullerene (IF) nanoparticles (Fig. 9) [38–40]. In a typical synthesis, the fluoride colloidal nanoparticles were hydrothermally treated at a temperature range of 80–180 °C. The formation of IF nanoparticles seems to be related to the hexagonal structures, since IF nanoparticles were only found in the samples of lanthanide fluorides that possessed hexagonal crystal structures: LaF_3, PrF_3, NdF_3, and SmF_3. In the orthorhombic YF_3, fewer IF nanoparticles were observed. The size of these IF nanoparticles is flexible to some extent; temperature and molar ratio have been found to be responsible for the size and shape control of these nanostructures.

Compared with the reported IF/nanotube nanostructures, rare-earth fluorides and hydroxides have no typical layer structures. However, it seems that the closed-cage structures are also thermodynamically stable for these fluorides and hydroxides. Based on experimental results, we believe that the rare-earth fluorides and hydroxides may not be regarded as typical 3D compounds, and may be the structural intermediates between 3D and 2D structures [38–40]. Similar phenomena have been observed and confirmed by Tenne and Rao et al. in the subsequent synthesis of non-layer HfS hollow nanoparticles [51]. However, a clear explanation of the structural rational of these IF nanostructures may need a thorough theoretical and structural investigation.

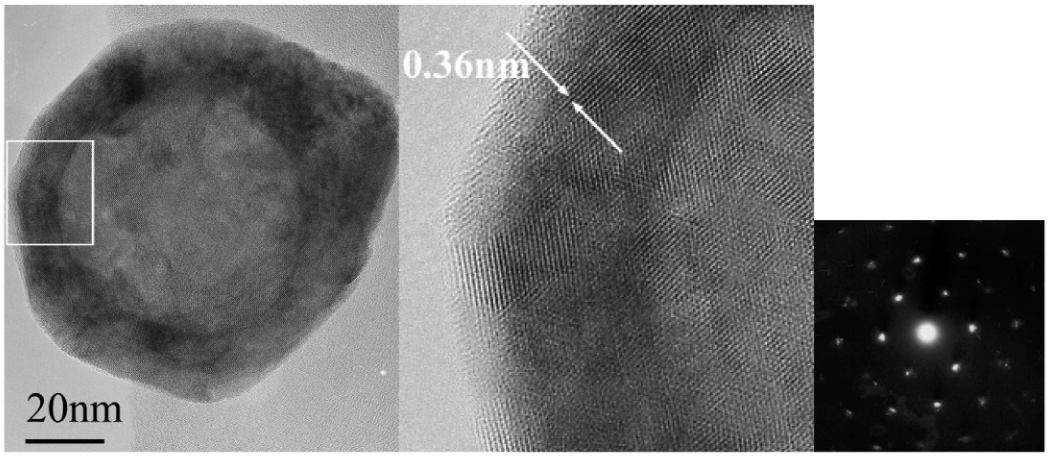

Fig. 9 (A) An individual LaF_3 IF nanoparticle with diameter ~90 nm; (B) magnification of the square section shown in A; (C) electron diffraction pattern of the IF nanoparticle in A (adapted from [38]).

Stemming from an aqueous solution, these hydroxide nanotubes/nanowires are sure to have unique hydrophilic properties, and may serve as effective confined templates for 1D nanostructures (Fig. 10). The morphologies of these tubular or nanowire structures can be maintained even after thermal treatment at 700 °C; however, a dehydration process will occur and result in the formation of oxide nanotubes/nanowires. Another treatment mode will lead to the formation of oxysulfide nanotubes/nanowires if the hydroxide ones were mixed with sulfur to form a homogenous mixture, and then treated at a temperature ~700 °C under the protection of Ar (or N_2) atmosphere. Also, F-substituted hydroxide nanotubes can be prepared. Our experiments have shown that, based on a simple hydrothermal method and with hydroxides as possible precursors, different kinds of rare-earth compound nanotubes could be easily obtained, and the great flexibility of rare-earth chemistry has been utilized in generating various rare-earth compound nanomaterials.

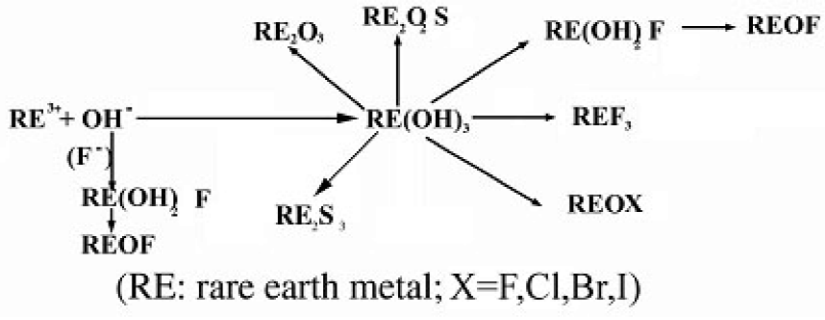

Fig. 10 Conversion of rare-earth hydroxides into rare-earth compounds nanostructures.

Based on the hydrophilic properties of the rare-earth nanotubes/nanowires, we have developed a general method for their further functionalization in aqueous solution. For example, the hydrophilic outer surface of these nanotubes could be modified with metal nanoparticles: by immersing $Y(OH)_3$ nanotubes into aqueous hydrazine solution, then into Ag^+ (or Au^{3+}, etc.) solutions, these nanotubes could be coated with Ag (or Au, etc.) nanoparticles (Fig. 8). Another facile functionalization process

has been demonstrated by simply immersing the $Y(OH)_3$ nanotubes into 0.04 mol/l Eu^{3+}, or Yb^{3+}/Er^{3+} (Er:Yb = 1:6) aqueous solutions, and the subsequent sulfuration process leads to the formation of doped oxysulfide nanotubes.

This chemical modified method has been further proved to be a facile functionalization method by the up- and down-conversion luminescence experimental results.

The hydrophilic properties of the rare-earth nanotubes/nanowires have also enabled the possibilities of preparation of inorganic–organic rare-earth nanostructures (Fig. 11) [52]. Generally, functional molecules with ester groups can be used in this process. Methyl methacrylate (MMA) has been chosen as an example. The covalent functionalization involves the irreversible esterolysis of a bifunctional molecule, MMA, and the formation of Y(III)–O bonds on the hydrophilic surface of $Y(OH)_3$ nanotubes (YNTs) in water. This leads to amphipathic composite nanotube synthesis by attachment of carbon–carbon double-bond chains to YNTs without disrupting the original structure (Fig. 11). Both the forming of the YNTs and C=C attachment were achieved in a single step.

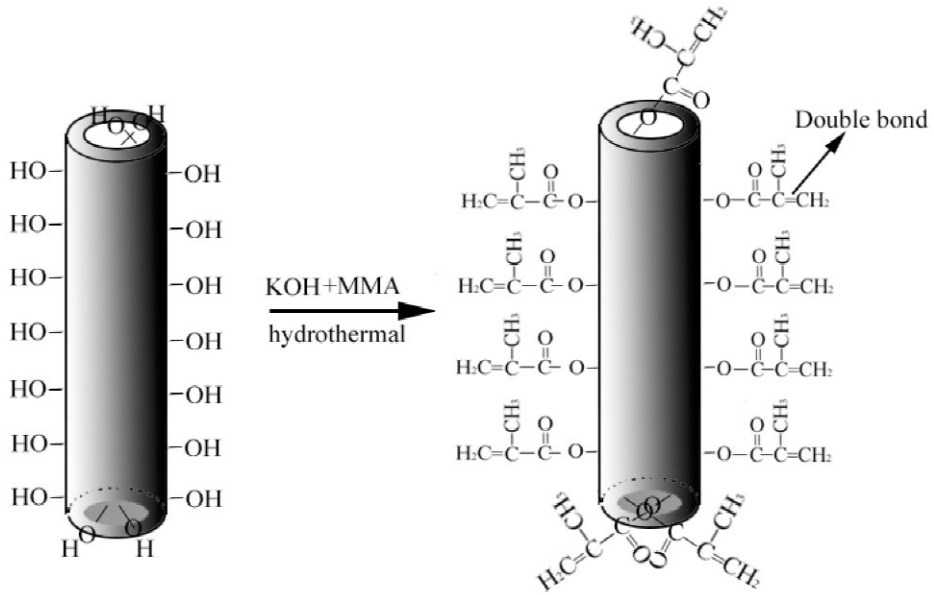

Fig. 11 Schematic of $Y(OH)_3$ nanotubes formation and subsequent grafting of carbon–carbon double-bonds (adapted from [52]).

In this section, by effectively tuning the chemical potentials in the aqueous system, a new chemical synthetic strategy has been established to synthesize series of rare-earth nanowires, nanotubes, and IF-like new-type nanostructures, which greatly enriched the categories of low-dimensional nanostructures. Different chemical reactions, such as dehydrate, sulfuration, etc., have been applied to generate various rare-earth compound nanostructures, during which the great flexibility of rare-earth chemistry has been utilized in generating various rare-earth compound nanomaterials. Based on the experiment results, the nanotubes have been obtained at a lower-temperature condition than that of the nanowires, and the structure transitions from rare-earth nanotubes to nanowires have been investigated in detail in different rare-earth systems. A similar rolling mechanism to that of the MnO_2 system has been established to guide the growth of these rare-earth low-dimensional nanostructures, which shows the generality of this mechanism. Based on the successful synthesis of these nanostructures, some preliminary optical properties have been investigated. Owing to the interesting combination of novel nanostructures

and functional compounds [53–55], these rare-earth low-dimensional nanostructures can be expected to bring some new opportunities in vast research areas and application in biology, catalysts, and optoelectronic devices.

SILICATE NANOTUBES AND NANOWIRES

This proposed rolling mechanism has also been evidenced in the silicate series [42–43]. A water–ethanol mixed-solution hydrothermal route has been developed to prepare a series of silicate nanowires and nanotubes, based on the chains and layer structures of silicates, respectively.

The silicates are the largest, most interesting, and most complicated class of minerals by far. Approximately 30 % of all minerals are silicates, and 90 % of the Earth's crust is made up of silicates. The basic unit of silicates is the (SiO_4) tetrahedron-shaped anionic group with a –4 charge, which can be linked to each other in different modes and form as single units, double units, chains, sheets, rings, and framework structures. In the layer-structured subclass, hexagon rings of tetrahedrons are linked by shared oxygens to other rings in a 2D plane (Fig. 12) [56]. The silicon-to-oxygen ratio is generally 1:2.5 (or 2:5) because only one oxygen is exclusively bonded to the silicon and the other three are half-shared (1.5) with others. Linus Pauling pioneered the study of the crystal structure of layered silicates, including micas and chlorite, and predicted that if the two crystal faces of a constituent layer of a layer crystal are not equivalent, there would be a tendency for the layer to curve, one face becoming concave and one convex, and this tendency would in general not be overcome by the relatively weak force operative between adjacent layers [57].

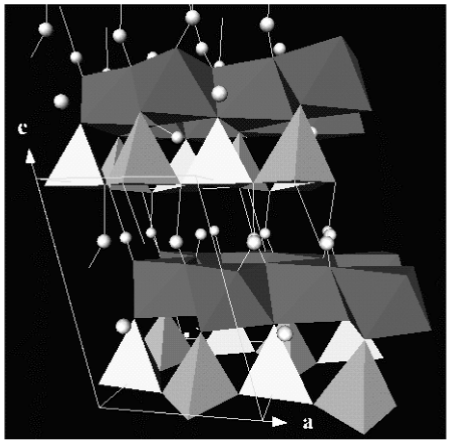

Fig. 12 Crystal structure of clay-type silicates.

Based on our experiment results [42], the as-obtained silicate nanotubes usually have clay-type structures (similar to that of kaolenite), which are composed of asymmetric alternating sheets of silica tetrahedron and metal oxide octahedron. So it is believed that the growth of these silicate nanotubes is based on the asymmetry along the *c*-axis of the layered metal silicates (Fig. 13).

The synthesis of silicate nanotubes was based on a hydrothermal method in a mixed-solution system. Although the silicates may have layer structures in nature, the direct reaction of metal ions and Na_2SiO_3 in water only results in irregular particles. As mentioned in the preparation of MnO_2 nanotubes, the formation of nanotubes may need some desirable conditions to facilitate the exfoliation process of the layers. Our experiments show that a water–ethanol mixed solution is the optimal condition.

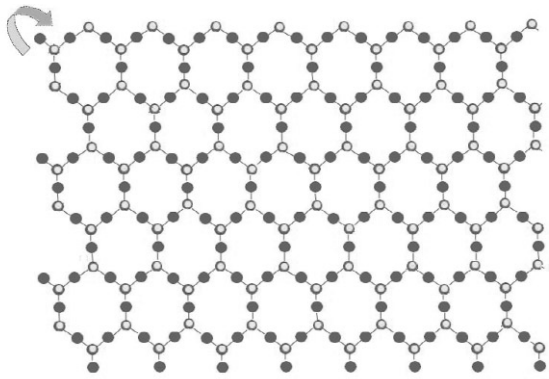

Fig. 13 Rolling mode of silicate nanotubes.

As shown in Fig. 14, all kinds of silicates can be prepared as uniform nanotube morphologies with open ends, which enable them with possible applications in gas absorption/separation and catalysis fields. For different interlayer cations, the silicate nanotubes have different diameters possibly due to the difference in interaction between layers and the subsequent difference in the rigidity of the silicate sheets, for example, copper silicate nanotubes have diameters 8~10 nm and lengths up to hundreds of nanometers (Fig. 14A), while that of magnesium (Fig. 14B), calcium (Fig. 14D), and cadmium (Fig. 14E) silicates have diameters 15~20 nm and length up to 1 μm. Due to the excellent ion-exchange characteristics of layered silicates, cations residing between the layers can be further replaced, which make these nanotubes ideal candidates as molecular seives.

The as-obtained nanotubes have tunable nanometer-scale pore sizes, narrow size distributions, and large Brunauer–Emmett–Teller (BET) surface areas, and have shown excellent catalytic oxidation performance at low-temperature range and a hydrogen storage capacity of up to 1.8 % at room temperature [42]. Compared with the well-known mesoporous materials, the as-obtained nanotubes have shown better thermal/hydrothermal stabilities, and, compared with the zeolites, these nanotubes have larger pores, which can satisfy the requirement in catalytic synthesis of macromolecules [58–65].

Silicates have silicate-oxygen tetrahedral as their basic structural units, and different link modes will lead to the formation of different structures of silicates. Other distinctive structures are the chain-like silicates with a Si:O = 1:3 when tetrahedral are connected to each other in a linear way, which may be favorable for the anisotropic growth. It is believed that the formation of these nanowires is closely related to this particular link mode [43,65].

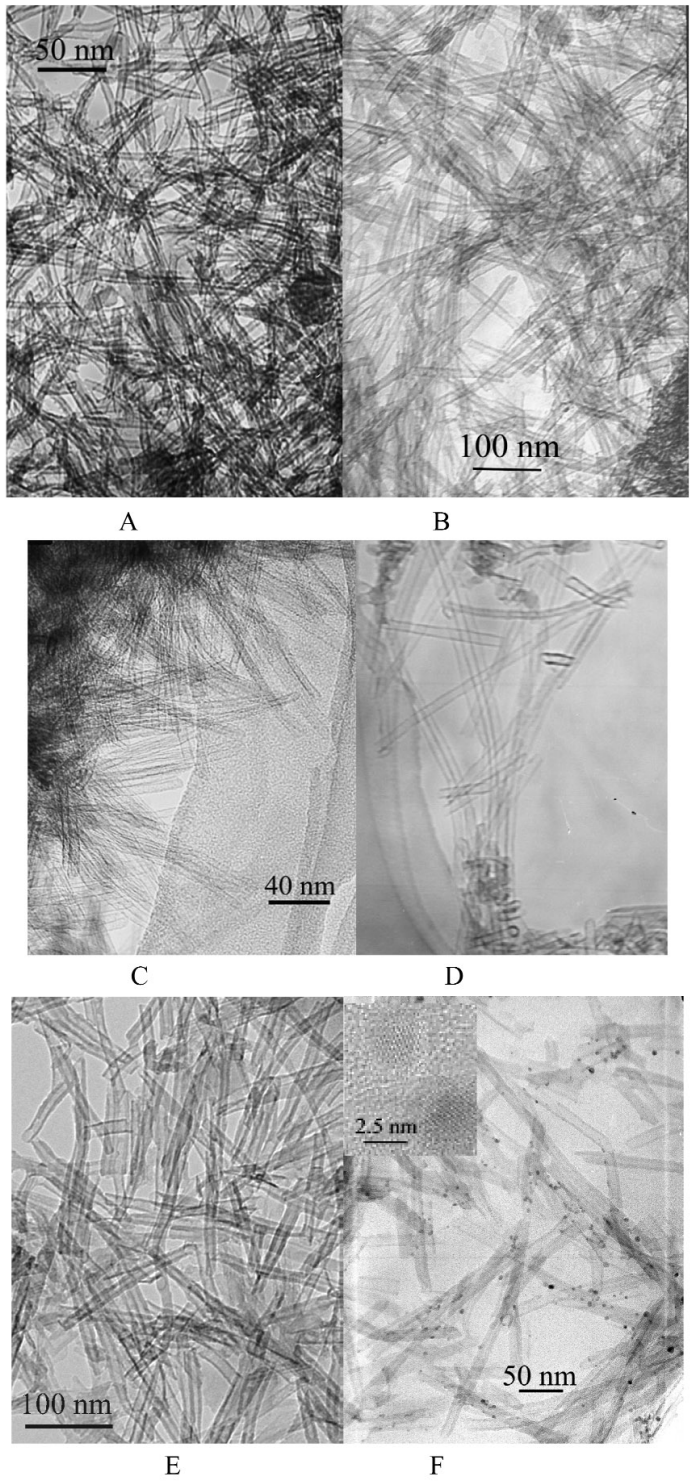

Fig. 14 (A) TEM images of $CuSiO_3 \cdot 2H_2O$ nanotubes; (B) TEM images of $Mg_3Si_2O_5(OH)_4$ nanotubes; (C) TEM images of barium silicate nanotubes; (D) TEM images of calcium silicate nanotubes; (E) TEM images of cadmium silicate nanotubes (adapted from [42]); (F) Pd-doped $Mg_3Si_2O_5(OH)_4$ nanotubes.

As stimulated by the successful synthesis of nanotubes from layered silicates, this water–ethanol hydrothermal route has been applied to the synthesis of silicate nanowires. By simply tuning several parameters, such as temperature, concentration, water–ethanol ratios, etc., the crystal structure and growth behavior of nanocrystals can be easily modulated and several kinds of silicate nanowires, such as calcium, strontium, barium, zinc, and cadmium silicates, etc., have been successfully prepared (Fig. 15).

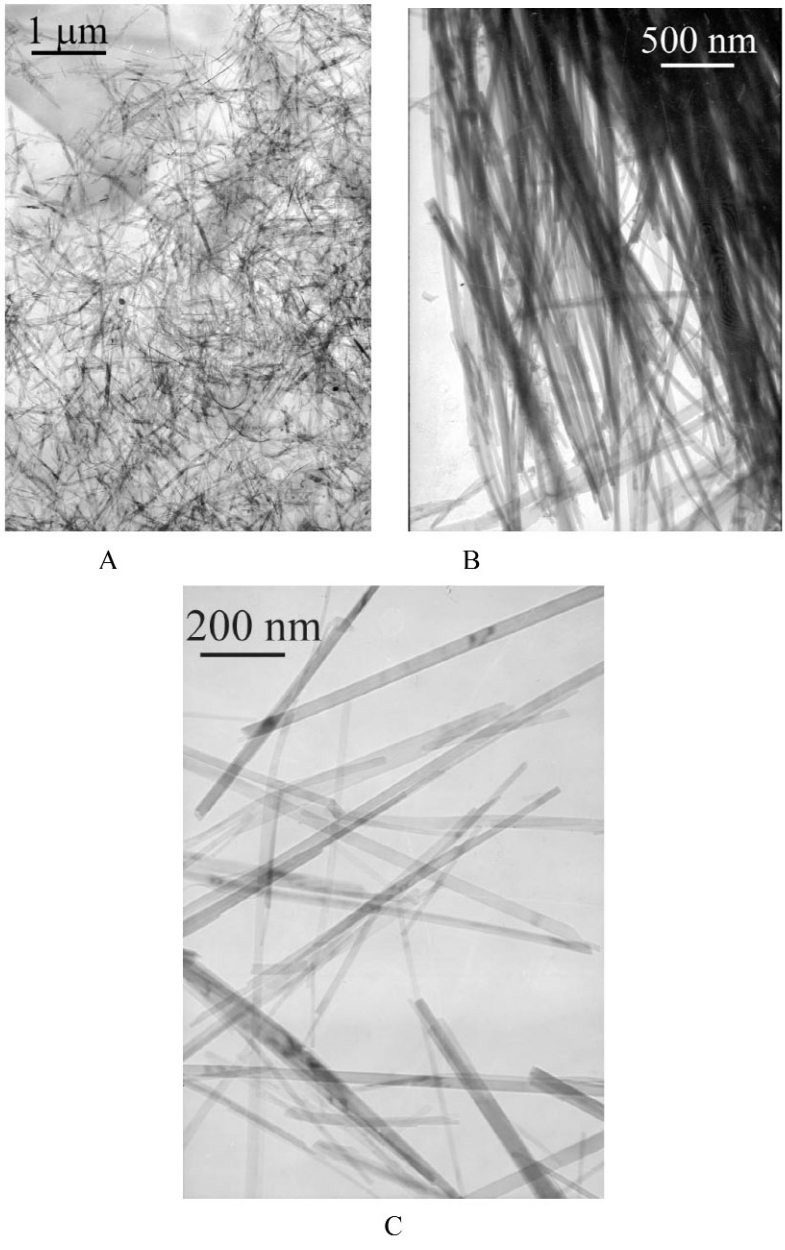

Fig. 15 (A) TEM images of sodium calcium silicate nanowire; (B) TEM images of $SrSi_3O_9$ nanowires; (C) TEM images of $Na_2Cd_3(Si_3O_{10})$ nanowires (adapted from [43]).

Silicate compounds are usually characteristic of affluent crystal structure and compositions. So it still remains a challenge to exactly control the growth behavior and morphology of the silicates. Nevertheless, this water–ethanol mixed-solution synthetic route has shown some potential in designed synthesis. Undoubtedly, the crystal structures of the final products are important factors that should merit particular attention, and in the case of silicate nanotubes, the underlying principle is the rolling mechanism from layer structures to nanotubes.

SUMMARY AND PERSPECTIVE

In this dissertation, three systems of MnO_2, rare-earth compounds, and silicates have been chosen to illustrate the methodology in controlled synthesis of 1D TMO nanostructures under aqueous synthetic conditions. Various chemical reactions such as redox, precipitation, complexation reaction, etc., have been widely employed in the investigation of the controlled growth of TMO 1D nanostructures, and shown amazing abilities in yielding new nanostructures with designed compositions, dimensionalities, and crystal structures. As the main task of chemistry, the creation of new molecular and new materials will bring us many more opportunities than ever, and will always be the central topic of science.

There is a bright future for the controlled synthesis of nanostructures and nanomaterials. Specifically, the advances in the controlled synthesis of nanostructures are just a beginning. The underlying principle in shape and size control are far from satisfactory, which have proved important factors that will determined the properties of materials by more and more studies. Further investigation can focus on the establishment of general synthetic methodology [66], which may be central to making progress toward designed synthesis according to demands.

REFERENCES

1. <http://www.zyvex.com/nanotech/feynman.html>
2. A. P. Alivisatos. *Science* **271**, 933–937 (1996).
3. X. G. Peng. *Adv. Mater*. **15**, 459–463 (2003).
4. J. T. Hu, T. W. Odom, C. M. Lieber. *Acc. Chem. Res*. **32**, 435–445 (1999).
5. S. R. Forrest. *Chem. Rev*. **97** (6), 1793–1896 (1997).
6. Y. N. Xia, P. D. Yang, Y. G. Sun, Y. Wu, B. Mayers, B. Gates, Y. Yin, F. Kim, H. Yan. *Adv. Mater*. **15**, 353–389 (2003).
7. X. Duan, Y. Huang, Y. Cui, J. Wang, C. M. Lieber. *Nature* **409**, 66 (2001).
8. Y. Cui and C. M. Lieber. *Science* **291**, 851 (2001).
9. Y. Huang, X. Duan, Y. Cui, L. Lauhon, K. Kim, C. M. Lieber. *Science* **294**, 1313 (2001).
10. J. Goldberger, R. He, Y. Zhang, S. Lee, H. Yan, H.-J. Choi, P. Yang. *Nature* **422**, 599–602 (2003).
11. Z. W. Pan, Z. R. Dai, Z. L. Wang. *Science* **291**, 1947–1949 (2001).
12. X. Y. Kong, Y. Ding, R. Yang, Z. L. Wang. *Science* **303**, 1348–1351 (2004).
13. T. J. Trentler, K. M. Hickman, S. C. Goel, A. M. Viano, P. C. Gibbons, W. E. Buhro. *Science* **270**, 1791–1794 (1995).
14. Y. G. Sun, B. Gates, B. Mayers, Y. Xia. *Nano. Lett.* **2**, 165–168 (2002).
15. G. Sun and Y. N. Xia. *Science* **298**, 2176–2179 (2002).
16. Y. D. Li, J. W. Wang, Z. X. Deng, Y. Wu, X. Sun, D. Yu, P. Yang. *J. Am. Chem. Soc.* **123**, 9904–9905 (2001).
17. J. W. Wang and Y. D. Li. *Adv. Mater*. **15**, 445–447 (2003).
18. Y. D. Li, X. L. Li, R. R. He, J. Zhu, Z. X. Deng. *J. Am. Chem. Soc.* **124**, 1411–1416 (2002).
19. Y. D. Li, X. L. Li, Z. X. Deng, B. Zhou, S. Fan, J. Wang, X. Sun. *Angew. Chem., Int. Ed.* **41**, 333–335 (2002).
20. X. M. Sun and Y. D. Li. *Chem. Eur. J.* **9**, 2229–2238 (2003).
21. X. M. Sun, X. Chen, Y. D. Li. *Inorg. Chem.* **41**, 4996–4998 (2002).

22. X. Chen, X. M. Sun, Y. D. Li. *Inorg. Chem.* **41**, 4524–4530 (2002).
23. X. L. Li, J. F. Liu, Y. D. Li. *Inorg. Chem.* **42**, 921–924 (2003).
24. M. H. Huang, S. Mao, H. Feick, H. Yan, Y. Wu, H. Kind, E. Weber, R. Russo, P. Yang. *Science* **292**, 1897–1899 (2001).
25. M. Law, D. J. Sirbuly, J. C. Johnson, J. Goldberger, R. J. Saykally, P. Yang. *Science* **305**, 1269–1273 (2004).
26. M. Law, H. Kind, B. Messer, F. Kim, P. Yang. *Angew Chem., Int. Ed.* **41** (13), 2405–2408 (2002).
27. N. G. Chopra, R. J. Luyken, K. Cherry, V. H. Crespi, M. I. Cohen, S. G. Louie, A. Zettl. *Science* **269**, 996 (1995).
28. (a) R. Tenne. *Adv. Mater*. **7**, 965 (1995); (b) R. Tenne, L. Margulis, M. Genut, G. Hodes. *Nature* **360**, 444 (1992); (c) R. Tenne. *Chem. Eur. J.* **8**, 5297 (2002).
29. Y. R. Hachohen, E. Grunbaum, J. Sloan, J. L. Hutchison, R. Tenne. *Nature* **395**, 336 (1998).
30. M. E. Spahr, P. Bitterli, R. Nesper, M. Müller, F. Krumeich, H.-U. Nissen. *Angew. Chem., Int. Ed.* **37**, 1263 (1998).
31. D. Ugarte. *Nature* **359**, 707 (1992).
32. Z. X. Deng, L. B. Li, Y. D. Li. *Inorg. Chem.* **42**, 2331 (2003).
33. X. Wang and Y. D. Li. *J. Am. Chem. Soc.* **124**, 2880–2881 (2002).
34. X. Wang and Y. D. Li. *Chem. Commun.* 764–765 (2002).
35. X. Wang and Y. D. Li. *Chem. Eur. J.* **9**, 300–306 (2003).
36. X. Wang and Y. D. Li. *Chem. Lett.* **33**, 48–49 (2004).
37. X. Wang and Y. D. Li. *Angew. Chem., Int. Ed.* **41**, 4790–4793 (2002).
38. X. Wang and Y. D. Li. *Angew. Chem., Int. Ed.* **42**, 3497–3500 (2003).
39. X. Wang, X.-M. Sun, D. Yu, B.-S. Zou, Y. Li. *Adv. Mater.* **15**, 1442–1445 (2003).
40. X. Wang and Y. D. Li. *Chem. Eur. J.* **9**, 5627–5635 (2003).
41. X. Wang, J. Zhuang, Y. D. Li. *Eur. J. Inorg. Chem.* 946–948 (2004).
42. X. Wang, J. Zhuang, J. Chen, K. B. Zhou, Y. D. Li. *Angew. Chem., Int. Ed.* **43**, 2017–2020 (2004).
43. X. Wang, J. Zhuang, Q. Peng, Y. D. Li. *J. Solid State Chem*. **178**, 2332–2338 (2005).
44. M. M. Thackeray. *Prog. Solid. State. Chem.* **25**, 1–71 (1997).
45. S. Ching, E. J. Welch, S. M. Hughes, A. B. F. Bahadoor, S. L. Suib. *Chem. Mater.* **14**, 1292–1299 (2002).
46. S. Ching, J. L. Roark, N. Duan, S. L. Suib. *Chem. Mater.* **9**, 750–754 (1997).
47. S. Ching, J. A. Landrigan, M. L. Jorgensen. *Chem. Mater.* **7**, 1604–1606 (1995).
48. A. Perner, K. Holl, D. Ilic, M. Wohlfahrt-Mehrens. *Eur. J. Inorg. Chem*. **5**, 1108–1114 (2002).
49. A. R. Armstrong and P. G. Bruce. *Nature* **381**, 499–500 (1996).
50. Z. R. Tian, W. Tong, J. Y. Wang, N.-G. Duan, V. V. Krishnan, S. L. Suib. *Science* **276**, 926–930 (1997).
51. M. Nath, C. N. R. Rao, R. Popovitz-Biro, A. Albu-Yaron, R. Tenne. *Chem. Mater.* **16**, 2238 (2004).
52. W. J. Li, X. Wang, Y. D. Li. *Chem. Commun*. **2**, 164–165 (2004).
53. Y. Hasegawa, T. Ohkubo, K. Sogabe, Y. Kawamura, Y. Wada, N. Nakashima, S. Yanagida. *Angew. Chem., Int. Ed.* **39**, 357–360 (2000).
54. Y. Hasegawa, S. Thongchant, Y. Wada, H. Tanaka, T. Kawai, T. Sakata, H. Mori, S. Yanagida. *Angew. Chem., Int. Ed.* **41**, 2073–2075 (2002).
55. J. W. Stouwdam and F. C. J. M. van Veggel. *Nano. Lett.* **2**, 733–737 (2002).
56. D. T. Griffen. *Silicate Crystal Chemistry*, Oxford University Press, New York (1992).
57. L. Pauling. *Proc. Natl. Acad. Sci. USA* **16**, 578–582 (1930).
58. A. Corma. *Chem. Rev.* **97**, 2373 (1997).
59. R. M. Hazen, R. T. Downs, L. W. Finger. *Science* **272**, 1769 (1996).

60. J. S. Beck, J. C. Vartuli, W. J. Roth, M. E. Leonowicz, C. T. Kresge, K. D. Schmitt, C. T.-W. Chu, D. H. Olson, E. W. Sheppard, S. B. McCullen, J. B. Higgins, J. L. Schlenkert. *J. Am. Chem. Soc.* **114**, 10834 (1992).
61. D. Y. Zhao, J. L. Feng, Q. S. Huo, N. Melosh, G. H. Fredrickson, B. F. Chmelka, G. D. Stucky. *Science* **279**, 548 (1998).
62. Z. T. Zhang, Y. Han, L. Zhu, R. W. Wang, Y. Yu, S. L. Qiu, D. Y. Zhao, F. S. Xiao. *Angew. Chem., Int. Ed.* **40**, 1258 (2001).
63. P. D. Yang, D. Y. Zhao, D. I. Margolese, B. F. Chmelka, G. D. Stucky. *Nature* 396, 152 (1998).
64. T. Sun and J. Y. Ying. *Nature* **389**, 704 (1997).
65. R. R. Hao, X. Y. Fang, S. C. Niu. *Series of Inorganic Chemistry* (3), p. 212, Science Press, Beijing (1998).
66. X. Wang, J. Zhuang, Q. Peng, Y. D. Li. *Nature* **437**, 121–124 (2005).